



# Design and validation of a phantom for transcranial ultrasonography

Denis Leonov<sup>1,2</sup> · Maria Kodenko<sup>1,3</sup> · Daria Leichenko<sup>2</sup> · Anastasia Nasibullina<sup>2</sup> · Nicholas Kulberg<sup>4</sup>

Received: 8 January 2022 / Accepted: 17 March 2022 / Published online: 10 April 2022  
© CARS 2022, corrected publication 2022

## Abstract

**Purpose** Commercial medical ultrasound phantoms are highly specific as they simulate particular clinical scenarios. This makes them expensive to use in multi-target research and training. General approaches to human tissue and organ modeling are described in the manufacturing methodology, access to which is restricted by the manufacturer's trade secret. Our aim is to propose a reproducible methodology to design a head phantom for transcranial ultrasound training and research from widely available materials and to validate its applicability.

**Methods** To create an anthropomorphic phantom, we used data from real patients obtained by CT and MRI scans. We combined FDM and LCD 3D printing to achieve the desired acoustic performance and ergonomics of the phantom. We fabricated the phantom using polyvinyl chloride plastisol, photopolymer, and PLA to simulate brain tissue, temporal acoustic windows, and acoustically opaque parts of the skull, respectively. Notably, the phantom fabrication method uses only readily available materials and is easy to reproduce.

**Results** We developed a basic one and anatomical one versions of the head phantom. The basic version contains a simplified brain: tissue-mimicking material is poured into the skull with needles inserted, which specific pattern is easy to recognize in B-mode images. The anatomical version has an anatomically correct brain dummy extracted from MRI data and contains multiple randomly distributed small metal, plastic, and bony objects ranging in size from 1 to 3 mm each.

**Conclusion** The proposed methodology allows producing head phantoms for transcranial ultrasound training and research. The anatomical accuracy of the model is proved by ultrasonography and CT studies. Both versions of the phantom comprise the skull and the brain and are intended for ultrasound imaging through the temporal bone acoustic window. Needles and small objects serve as navigation targets during the training procedure. The basic version helps learning basic navigation skills, while the anatomical one provides a realistic setting to perform the diagnostic procedure.

**Keywords** Transcranial sonography · Tissue-mimicking material · Three-dimensional printing · Brain phantom · Medical training · Head phantom

## Introduction

Phantoms of various types are widely used to calibrate medical devices, develop and test imaging algorithms, teach and train healthcare professionals, and plan surgical interventions (e.g., the literature describes the design of head

phantoms [1–3] intended to test systems for high-intensity ultrasound therapy of the brain). Phantom fabrication is commercialized by a number of companies (e.g., CIRS, SAE, Sun Nuclear, Kyoto Kagaku, etc.), but only True Phantom produces anatomically correct head models. However, in most instances, commercial medical ultrasound phantoms simulate just one of many particular clinical scenarios. This makes them expensive to use in multi-target research and training. Moreover, in the present literature, there are no papers that focus on the design of transcranial ultrasound imaging phantoms.

The intended use determines the following set of requirements for a phantom of this type. It should be easy to manufacture, durable, safe, easy to use, and comparable to the simulated object, which means that the acoustic

✉ Denis Leonov  
strat89@mail.ru

<sup>1</sup> Moscow Center for Diagnostics and Telemedicine, Moscow, Russia

<sup>2</sup> Moscow Power Engineering Institute, Moscow, Russia

<sup>3</sup> Bauman Moscow State Technical University, Moscow, Russia

<sup>4</sup> Federal Research Center “Computer Science and Control”, Moscow, Russia

properties of a simulator should correspond to those of the real object. Agar-gelatin mixtures are commonly used for soft-tissue mimicking [4, 5] as the characteristic speed of sound in them is comparable to that in soft tissues and lies in the range of 1498–1600 m/s, while necessary attenuation and scattering values can be obtained with the introduction of additives. However, this material is not durable and requires special storage conditions. Bone tissue is mimicked by PLA [6], a plastic that is widely used in 3D printing by fused deposition modeling. The main drawback of this modeling technique is air gaps between the layers that introduce unrealistically high attenuation of ultrasound and make the models unsuitable for diagnostic sonography.

Thus, commercial medical ultrasound phantoms are highly specific and expensive. General approaches to human tissue and organ modeling are described in the manufacturing methodology, access to which is restricted by the manufacturer's trade secret. The aim of this work is to propose and validate a reproducible technique to fabricate anatomically correct training and research phantoms for diagnostic transcranial ultrasonography from widely available materials.

## Materials and methods

### Ultrasound scanner

The study used Medison Sonoace 8000 EX Prime, a medical ultrasound device with a C3-7ED convex probe with an aperture width of 70 mm and a P2-5AC sector phased-array probe with an aperture width of 19 mm. The operating frequency was set to 5 and 3.5 MHz for convex and phased-array probes, respectively.

### 3D printers

We used Picaso 3D Designer X Pro FDM printer and Phrozen Shuffle 4 K LCD printer with an ultraviolet  $3940 \times 2160$  pixel matrix which gives the resolution of up to  $31 \mu\text{m}$ . The Phrozen printer operates at a wavelength of 405 nm, with a layer thickness of  $10 \mu\text{m}$ , and prints objects of no more than  $68 \times 120 \times 170$  mm at a speed of 30 mm/h. The Picaso printer has a heated table and closed build chamber with a print area of  $200 \times 200 \times 210$  mm and a layer thickness of  $50 \mu\text{m}$ , which is optimal for professional 3D modeling. The Picaso printer can work with two plastics simultaneously, which means that water-soluble support material can be used.

### Soft-tissue mimicking material

We used polyvinyl chloride plastisol as the main substance for soft-tissue mimicking. However, pure plastisol is transparent to ultrasound and needs an additive to increase the

dispersion coefficient. In our preliminary experiments, we investigated the effect of adding zinc oxide and titanium dioxide on the attenuation of ultrasound in polyvinyl chloride plastisol. Both additives are easy to use and freely available on the market. It turned out that, given the same concentration in relation to polyvinyl chloride plastisol, zinc oxide caused lower attenuation of ultrasound waves in the medium compared to titanium dioxide. Hence, with zinc oxide, the control of attenuation values was more precise. We experimented with different concentrations and found that the mixture of 0.4% zinc oxide with plastisol allowed observing a sonogram that resembled in vivo ultrasound images of the human brain. Thus, to mimic brain tissues, we used a mixture of polyvinyl chloride plastisol (99.6%) and zinc oxide (0.4%).

### 3D printing materials

To select the material, a study was conducted during which samples of materials commonly used in 3D printing, e.g., photopolymer resin, ABS, HIPS, SBS, PETG, PVA, PLA, BFWood, BFNylon, Ceramo, Watson, and Flex, were placed in frozen plastisol. A week later, ABS, SBS, HIPS, and Watson were found to be completely dissolved, so they were considered unsuitable for making molds for plastisol casting and storage.

To simulate temporal windows of the skull, photopolymer resin, an acoustically transparent material, and printing by LCD photolithography were used as this printing technique has high accuracy ( $31 \mu\text{m}$ ) and a 100% infill due to the fact that the model is always immersed in the liquid resin during printing. A sample printed by LCD photolithography has ultrasonic transparency close to that of bone tissue, while the materials used in FDM printing were found to be opaque to ultrasound. To find the appropriate material for modeling, we experimented with Industrial Blend (IB), Standard Blend (SB), SB black, SB red (Fun To Do, Netherlands), Flex HL (Hardlight, Russia), and Flex GL (Gorky Liquid, Russia) resins. The rest of the skull was printed from PLA plastic using water-soluble support material. We also used PLA to print casting molds as this material withstands relatively high temperatures and does not interact chemically with polyvinyl chloride plastisol.

### Manufacturing process

#### Skull model

To develop an anthropomorphic phantom, the skull model was extracted from a CT scan in Radiant DICOM Viewer using density filter; the CT scan at a bone window width of 500 to 2000 HU is shown in Fig. 1a. The resulting model was exported to Meshmixer to remove unwanted elements left after segmentation and divide the model into slices of

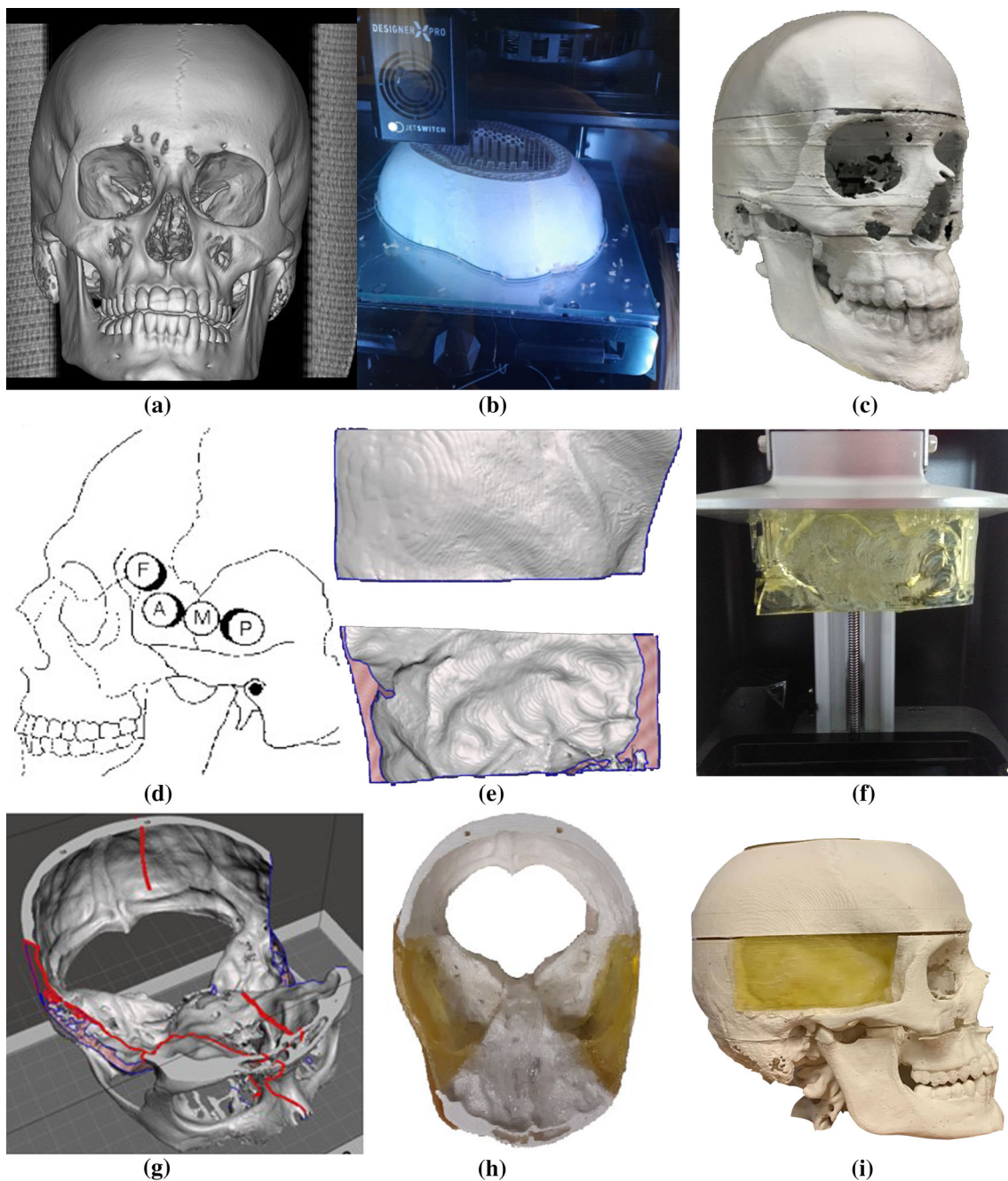


**Fig. 1** Skull model manufacturing process. **a** Bone segmentation on a CT scan. **b** FDM 3D printing of the phantom. **c** Assembled skull model. **d** Ultrasound phased array probe placement area. **e** Inner and outer sides of the virtual model of the temporal bone. **f** LCD printing of the temporal

bone model. **g** View of the central part of the phantom. **h** Printed central part of the phantom with the fixed acoustic windows. **i** Photograph of the assembled model

2–52 mm. The phantom is designed for ultrasound training and practice, so it was decided to divide the skull into 3 sections for step-by-step assembly with special fasteners. The prepared slices of the three-dimensional model were printed on Picaso 3D Designer X Pro using PLA plastic as shown in Fig. 1b, fastened together in sections, and covered with paint (Fig. 1c). It took about 24 h to print the largest slices.

### Acoustic windows

Usually, transcranial ultrasonography is performed through temporal acoustic windows (Fig. 1d) as this area is characterized by smooth and relatively thin bone tissue that gives the largest field of view [7]. Based on a CT scan, a virtual model of the temporal bone was built (Fig. 1e), and a sample shown

in Fig. 1f was printed by photolithography on the Phrozen printer.

To add acoustic windows, cutouts were made in the central part of the skull model (Fig. 1g). The acoustic windows were fixed in the printed model with a silicone sealant as shown in Fig. 1h. Finally, Fig. 1i demonstrates the phantom with the temporal acoustic window model after assembly.

### Making a simplified model of the brain

The bottom of the central part of the skull model was covered with foil, after which a mixture of plastisol heated to 160 °C and 0.4% ZnO was poured into it to model acoustic scattering. After cooling, the first group of steel pins with a diameter of 0.5 mm and a length of 25 mm was immersed in the tissue-mimicking material to serve as targets for ultrasound navigation when using the training phantom. After removing the foil, the second group of pins was placed counter to the first group in the lower part of the phantom section. Pins of both groups were placed according to individual patterns pre-selected for each group. This version of the phantom will be referred to as the basic one.

### Making an anthropomorphic model of the brain

The virtual model of the brain was derived from a magnetic resonance scan and is presented in Fig. 2a. After exporting from Radiant DICOM Viewer to Meshmixer, a mold was designed by subtraction from the cubic object. For ease of use, it was divided into three parts and equipped with fasteners as shown in photographs of the mold in Fig. 2b, c, and d. The two large parts of the mold are printed from light-colored plastic, and the third part is printed from gray plastic. The form was printed from PLA plastic by fused deposition modeling; the printing took about 100 h.

The two large parts of the mold were coupled and fastened together with adhesive tape and a layer of silicone sealant. The casting material was a mixture of polyvinyl chloride plastisol and zinc oxide; aluminum, PLA, and bone-tissue objects of 1–3 mm were added to the liquid mixture in a total of 30 objects of each material. We placed aluminum, PLA, and bone-tissue objects inside the brain model for training and research purposes. After mold filling, the gray-plastic part was inserted: it displaced the excess volume of liquid tissue-mimicking material and formed the lower part of the brain model. After cooling the brain model, it was easily removed from the collapsible mold (Fig. 2e). To perform ultrasonography through the temporal acoustic window, the anthropomorphic model of the brain was placed in the skull model. This version of the phantom will be referred to as the anatomical one.

### Experimental procedure

To choose a suitable photopolymer resin for the temporal bone modeling, sound velocity and attenuation values were measured in various resins; for this purpose, 30 × 30 × 20 mm rectangular parallelepiped samples had been printed from IB, SB, SB black, SB red, Flex HL, and Flex GL resins. Measurements were taken with A1550 IntroVisor flaw detector (Acoustic Control Systems, Russia) and two S3568 probes with a center frequency of 2.5 MHz. The probes were placed coaxially to the sides of the parallelepiped, and measurements were taken twice, with 20 mm and 30 mm between the probe apertures; sound velocity  $c$  was estimated from the time of signal arrival:

$$c = \frac{l_1 - l_2}{t_1 - t_2}, \quad (1)$$

where  $l_1$  and  $l_2$  are the distances between the coaxially placed probes, they are equal to 20 and 30 mm, i.e., the length and width of the rectangular parallelepiped samples;  $t_1$  and  $t_2$  are time intervals between excitation and arrival of ultrasound pulses traveling through the samples. The probing pulse had an envelope with a Gaussian shape and a length of 5 cycles. Time was measured at the peak value of the envelope. Attenuation  $\alpha$  was calculated from the difference in the received signal amplitude between the two measurements:

$$\alpha = \frac{A_1 - A_2}{l_1 - l_2}, \quad (2)$$

where  $A_1$  and  $A_2$  are the received signal amplitudes for the two measurements. Measurements were taken in the frequency range of 1–5 MHz.

To estimate the aberrations introduced by the temporal bone model, an ultrasound study was performed in which the phased-array probe was first placed onto the surface of a Gammex 1430 LE Mini-Doppler Flow System calibration phantom containing objects intended to check resolution in the B-mode, and then, the temporal bone model was placed between the probe and the phantom surface. As a result, two sonograms were obtained and analyzed. In this analysis, we performed the visual observation of the sonograms, measured the broadening of the point spread functions produced by the reflection of ultrasound waves from the string targets inside the Gammex phantom, and assessed the aberrations by estimating the angle between the original set of vertical nylon strings and its pseudo image caused by the distorting layer.

The study of the head with pins was two-stage: the phased-array probe was placed onto the acoustic window pre-covered with ultrasound gel and, first, the upper part of the phantom was probed, and then the lower part of the phantom was studied. As a result, sonograms of two patterns were obtained.

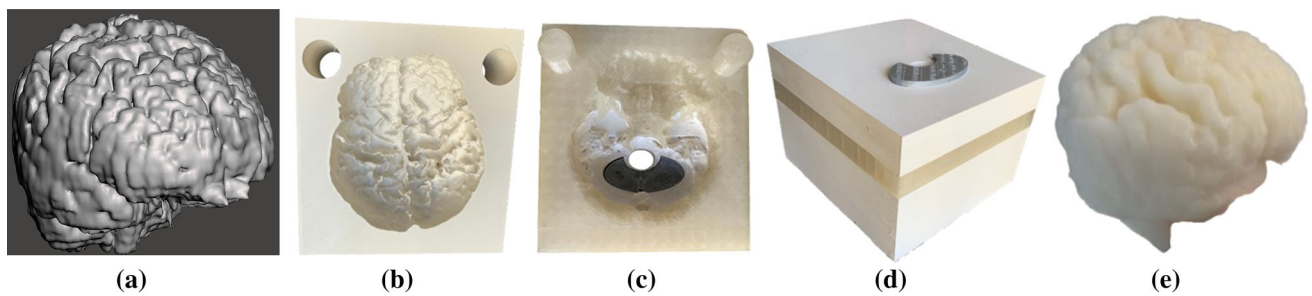


**Fig. 2** Manufacturing process of the anthropomorphic model of the brain. **a** Virtual model of the brain. **b** and **c** Parts of the mold. **d** Assembled mold. **e** Anthropomorphic model of the brain after removal from the mold

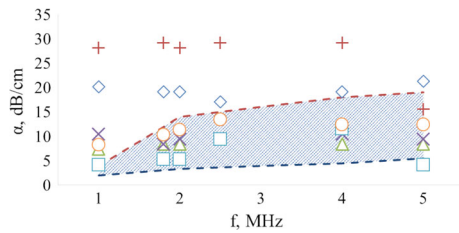


**Fig. 3** Frequency dependence of ultrasonic attenuation coefficient in the skull: (—) min, (---) max; and photopolymer resins: (◇) Flex GL, (+) SB, (△) SB black, (×) SB red, (□) IB, (○) Flex HL. The min and max values originate from [8] and correspond to the outer table and diploe, respectively

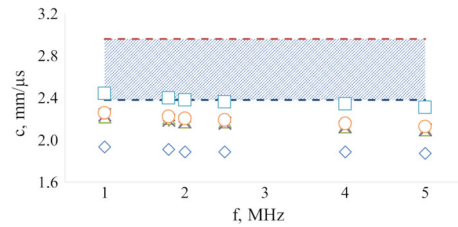


**Fig. 4** Frequency dependence of ultrasonic velocity in the skull: (—) min, (---) max; and photopolymer resins: (◇) Flex GL, (+) SB, (△) SB black, (×) SB red, (□) IB, (○) Flex HL. The min and max values originate from [8] and correspond to the outer table in different specimens

Ultrasonography of the anthropomorphic brain model was performed using the convex probe; for this study, the brain model was immersed in a container covered with sound-absorbing material and filled with degassed water; the study evaluated the brain contours, investigated particles in the B-mode, and measured the sound velocity.

The anthropomorphic dummy brain was placed in the skull model with temporal acoustic windows. Since the particles in the brain model were distributed randomly, their mapping was based on computed tomography of the phantom on Toshiba Aquilion 64 at a tube current of 350 mA and tube voltage of 120 kV. During ultrasonography of the head with the brain, ultrasound gel was applied to one of the acoustic windows, the probe was placed onto it, an ultrasound examination was performed, and a sonogram was recorded.

## Results

The study results are given in Figs. 3, 4, 5, 6, 7, 8 and 9. Figures 3 and 4 show experimental curves and the literature data for the skull bones. Obviously, attenuation values of IB, SB black, and SB red photopolymers and Flex HL are closest to that of the bone tissue, but only IB is comparable to it in terms of sound velocity, which is why it was chosen as the printing material for the temporal bone. The temporal bone model (Fig. 1f) was placed in the space between the

phased-array probe and the Gammex calibration phantom, and sonograms were taken in the presence and absence of aberrations as shown in Fig. 5a and b. It can be seen that the temporal bone model introduces distortions.

The basic version of the phantom (Fig. 6a) has target objects for transcranial ultrasonography training. Figure 6b and c demonstrate the external view of the central segment of the phantom with dark dots on a light background, i.e., the heads of pins. Figure 6d and e show sonograms of this phantom. It can be seen that ultrasound labels correspond to the upper and lower patterns in Fig. 6b and c; however, there are some specifics: (a) the size of the labels on the scanner screen is 3 mm, which is 6 times the diameter of the pins; (b) the pattern on the sonogram is slightly different from the pattern formed by the heads of pins.

The results of the anthropomorphic brain model study are illustrated in Fig. 7. The measured frequency dependence of the sound velocity in the brain tissue-mimicking material is shown in Fig. 8 along with the measurements for pure plastisol and dependency values derived from the literature.

During the manufacture of the anatomical version of the phantom, 30 metal and 30 bone-tissue particles were placed in the brain phantom. The frontal-plane location of particles in the phantom is illustrated by the CT scan in Fig. 9a. It can be seen that the particles did not settle down but were distributed evenly throughout the brain volume. Metal particles have a higher radiodensity (8000–19,000 HU) as compared

**Fig. 5** Studies of the temporal bone model with the Gammex phantom. **a** Sonogram of the phantom without distortion layer. **b** Sonogram of the phantom through the bone model

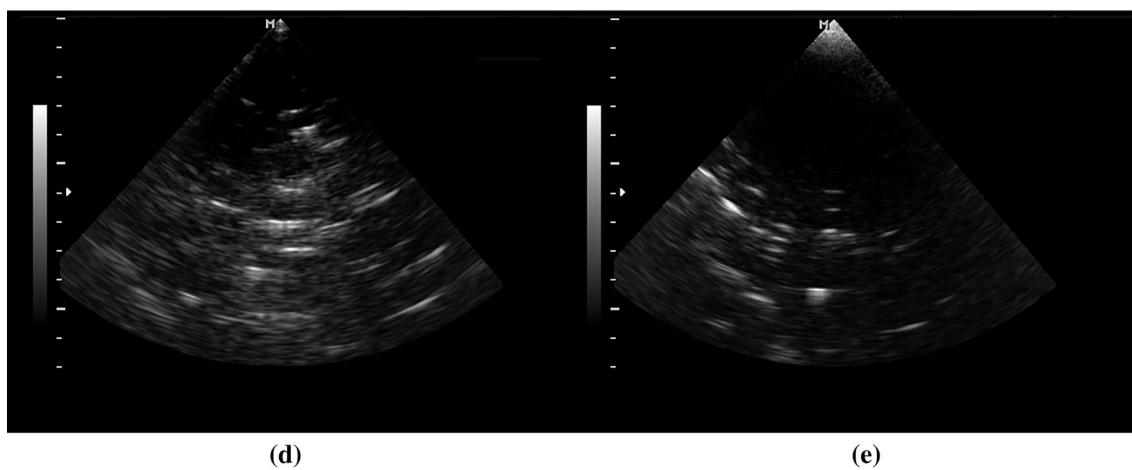
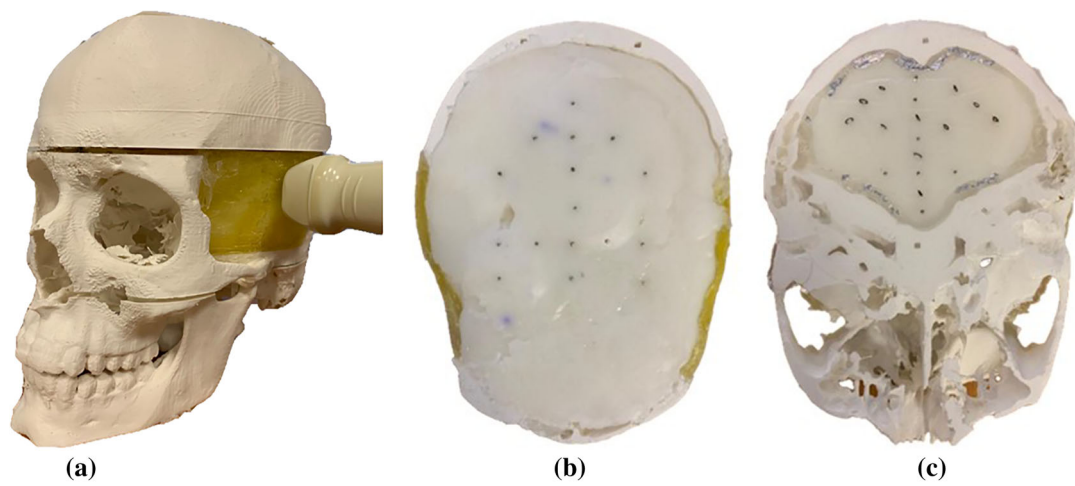
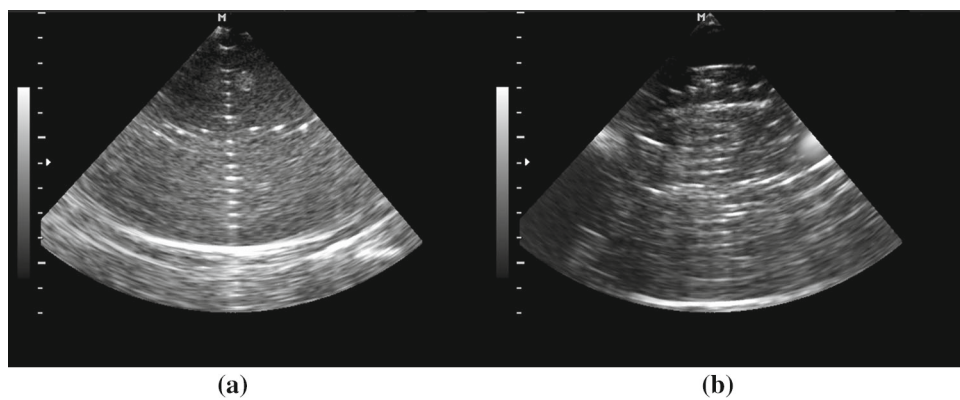


**Fig. 6** Studies of the basic version of the phantom. **a** View of the phantom with an ultrasonic probe placed onto the acoustic window. **b** Photograph of its central section taken from above. **c** Photograph of

the central section from below. **d** Sonogram of the central section of the phantom taken in the upper part. **e** Sonogram of the lower part. The bright dots in the sonograms represent the pins

**Fig. 7** Anthropomorphic brain model study. **a** Study process in which a researcher's hand holds a convex probe submerged in a water tank containing the brain model. **b** The image depicts a slice of the brain model in ultrasound

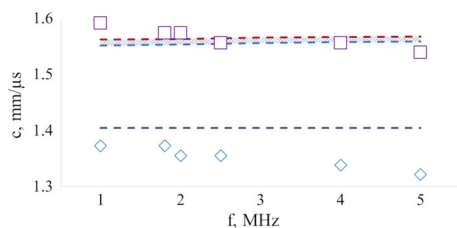
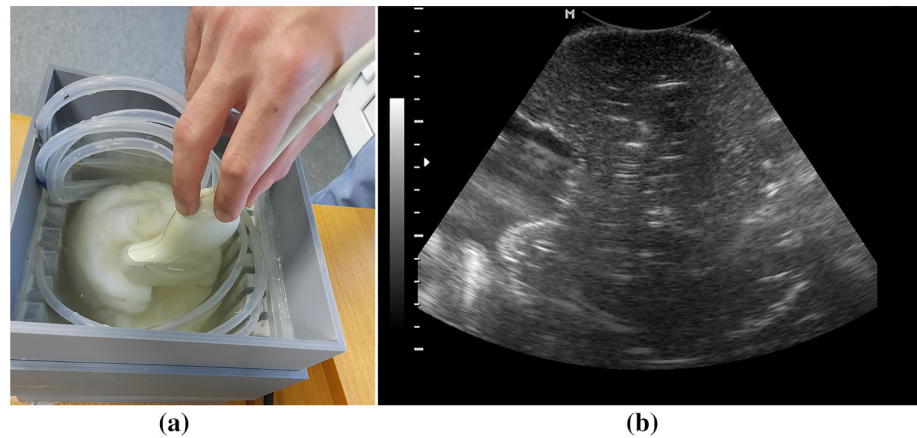


**Fig. 8** Frequency dependence of ultrasonic velocity in the brain in vitro (values originate from [9]): (---) min, (- - -) max; ( $\diamond$ ) pure plastisol in our experiments, ( $\square$ ) plastisol and zinc oxide mixture used for modeling the brain, and (- -) plastisol with hardener from [10]

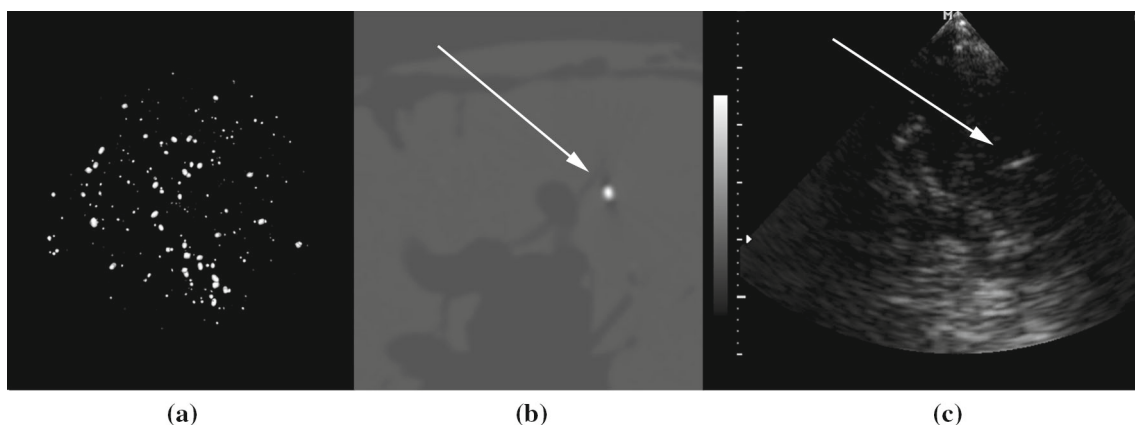
to bone-tissue particles (600–1500 HU). The phantom also contains PLA particles (100–190 HU), but they are not visible in Fig. 9a. The radiodensity of plastisol with a zinc oxide admixture is 60–100 HU.

Figure 9b shows a CT slice with the window settings based on the X-ray absorption coefficient for soft-tissue examination. The sonogram in Fig. 9c and the CT slice in Fig. 9b

demonstrate the same particle located 3 cm away from the skull; however, the size of the bright area corresponding to the particle on the sonogram is close to 5 mm and exceeds the actual size of the particle.

## Discussion

The proposed phantom meets the criteria for a training and demonstration model, i.e., it provides the possibility to train and compare the actual particle location and its display on the scanner screen. Anthropomorphic characteristics are obtained through the use of real patient data. Materials used in the phantom, i.e., PLA plastic, photopolymer resin, and polyvinyl chloride plastisol, have acceptable acoustic properties and are durable, wear-resistant, and chemically inert. Moreover, polyvinyl chloride plastisol is more durable than agar-agar or gelatin gel that is subject to drying and microbial contamination. Our measurements provided in Fig. 8



**Fig. 9** Study of the anatomical version of the phantom. **a** Three-dimensional reconstruction from a CT scan of the anatomical phantom model with metal and bone-tissue particles detected using the X-ray absorption coefficient. **b** CT slice of the region of interest with the

metal particle presented as the brightest area. **c** Sonogram of the same region of interest captured through the model of the temporal acoustic window. In CT and US images, the arrow points to the same metal target

showed that sound velocity in a pure material depends on the frequency and varies between 1320 and 1380 m/s, which does not exceed the literature data [10]; however, additives can increase sound velocity by about 200 m/s to achieve values comparable to those of the human brain [9]. In addition, Matheo et al. [10] stated that values may change over time; for example, in their experiment a year after fabrication, the attenuation coefficient of ultrasound at a frequency of 4.5 MHz in pure plastisol increased by 20.2%. Furthermore, Cabrelli et al. [5] and Carvalho et al. [11] noted that polyvinyl chloride plastisol reacts with plastics; in particular, it dissolves ABS plastic. Our experiments revealed that PLA plastic and photopolymer resin do not dissolve in plastisol, so these materials can be used together.

The choice of the material for temporal bone modeling is based on its similarity in terms of sound velocity and attenuation values to the bone tissue of the human skull [8]. According to Fig. 3 and 4, where min and max values originate from [8] and represent the real skull, Industrial Blend photopolymer resin (Fun To Do) was found to be the most similar material and was later used for modeling. Its sound propagation velocity was close to the lower limit of the outer table measured by Fry and Brager (1978) [8] in one of the specimens of the skull, while through all the other photopolymers in our experiment, sound traveled at significantly lower speeds. As for the sound pressure attenuation coefficient, Flex Gorky Liquid and Standard Blend photopolymer resins exceeded the upper limit measured for the diploe. Industrial Blend resin was well in between the diploe and outer table of the skull as measured in the range from 1.8 to 5 MHz.

The temporal bone model manufactured by LCD photolithography and used as an acoustic window was validated by the distortion analysis as seen in Fig. 5. The distortion values obtained in a B-mode study using the temporal bone model were compared to the distortions introduced by an *ex vivo* temporal bone model from our previous study [12]. Aberrations cause the probe beam to broaden [13], which results in the doubling of the line of string targets located perpendicular to the probe aperture. For an *ex vivo* object, the divergence angle between the true and false lines was  $13^\circ$  [12]. For the temporal bone model made of photopolymer resin, the divergence angle was  $15^\circ$ , which confirms its suitability. It is also worth noting that the introduction of the distorting layer led to a 1.5-time angular widening of the bright area corresponding to the string target located in the focal position in the sonogram.

Ultrasonography of the basic version showed an acceptable result, i.e., all elements of both patterns are clearly visible; the size of the pins on the scanner screen is 6 times larger than the actual one, which is due to the ultrasound device settings, phase aberrations and energy losses at the interface and when passing through the temporal bone model. The scanner settings matter since all devices are "by default"

intended for a specific model of the propagation medium with a sound velocity of 1540 m/s and a uniform attenuation equal to 0.7 or 1 dB/cm/MHz. The difference from this idealized model leads to incorrect estimation of the depth and size of labels. Moreover, the sonogram shows hyperechoic spots in places where there are no pins—these are punctures left after the pin removal. In the B-mode, they cannot be differentiated from pins. Nevertheless, one can touch the head of a pin with a finger and move it slightly, and such a movement will be reflected on the sonogram, which is impossible for punctures.

Previously, we have posted an archive [14] with STL files of the skull model and the brain mold. With these files, anyone can independently reproduce the phantom versions we developed.

For training using the basic version, we propose the following steps:

- (1) Take the assembled phantom and place an ultrasound sector probe onto the temporal acoustic window model as shown in Fig. 6a; ultrasound gel is applied to the probe.
- (2) Get an image of hyperechoic masses on the device screen as seen, for example, in Fig. 6d, and draw their location relative to each other.
- (3) Compare the drawing with the actual location of pins (Fig. 6b) looking from above at the central segment of the phantom.

Anatomical brain model study, which results are presented in Fig. 7, shows that the brain itself contains evenly distributed reflectors creating a homogeneous background. Against this background, multiple hyperechoic particles are visible, with some of them being 20 mm wide. It should be emphasized that the boundaries and typical anatomical contours of the brain model are clearly visible.

Transcranial ultrasonography of the anatomical version of the phantom proved the possibility of B-mode imaging differentiation between the brain, cranial tissues, and particles of metal, bone tissue, and PLA plastic. When examined through the temporal bone model, the size of particles in the sonogram exceeds the actual one by 3–10 times. The aluminum, PLA, and bone-tissue objects inside the brain model present an interest for training and research purposes. As for the training, the use of different materials reflects the difference in their CT and US appearance, i.e., the three materials are easily differentiated by windowing CT scans; at the same time, it is impossible to determine the particle material by means of ultrasound imaging. Thus, the phantom gives a better understanding of the specifics and capabilities of ultrasonography. As for the research, we have previously studied the appearance of ultrasound Doppler twinkling artifact upon various materials in agarose jelly and other mediums [15]. We believe that for future research, it is important to investigate



the appearance of the Doppler twinkling artifact in the head model. During testing in B-mode sonography, particles were not always visible against the background of tissues; in this case, our preliminary results demonstrate that the twinkling artifact can be used for their identification.

For training using the anatomical version of the phantom, we propose the following steps:

- (1) On a CT scan, select a slice where particles are visible.
- (2) Take the assembled phantom.
- (3) Apply gel to the surface of the temporal window model and place an ultrasound sector probe onto it.
- (4) On the ultrasound scanner screen, obtain a sonogram with a characteristic pattern of particles corresponding to the selected CT slice.
- (5) Based on the results of comparing the obtained sonogram and the selected CT slice, assess the transcranial ultrasonography competence of a trainee.

We practiced this training scheme and presented the pivot illustrations in Fig. 9. Figure 9a shows that there are plentiful targets inside the brain model. We chose one of the targets located close to the temporal acoustic window and found it in the CT slice as demonstrated in Fig. 9b. Then, with the sector probe, we found the same target during ultrasound examination and saved the corresponding sonogram (Fig. 9c). Note that the arrows in the CT scan and corresponding sonogram point to the chosen target. Thus, this successful exemplary demonstration allows to justify the applicability of the proposed phantom.

During manufacture, the following drawbacks of the process and the resulting phantoms were revealed:

- (1) Orbital and sinus bone tissues were not segmented enough, so they were missing in the corresponding places of the resulting skull model. This was overcome in [6], where painting tools were used to correct gaps in the segmentation of thin areas of the cranial bones. Another way to address this problem is to perform *ex vivo* imaging of the skull with no soft tissues.
- (2) When piercing plastisol with a pin, a trace is left that is hard to differentiate from the pin in the sonogram. When fabricating the model, such traces should be avoided as they mislead the trainee.
- (3) Parallelepiped PLA-plastic inserts printed on a 3D printer were used as fasteners for the assembly of skull model components. However, this proved impractical for repeated assembly and disassembly of the model. It would be more convenient to replace them with magnets.
- (4) In the fabrication process, polyvinyl chloride plastisol was used, which is known to have a lower sound velocity than brain tissues [10]: longitudinal elastic wave

propagation speed reaches 1560 m/s in brain tissues [4] and 1380 m/s in the soft-tissue mimicking mixture. X-ray absorption value is also different and amounts to 60–100 HU, while in brain tissues it is 40–55 HU, which imposes restrictions on the use of this material to create models for X-ray imaging.

- (5) Doppler color flow mapping of cerebral blood vessels cannot be performed on the presented phantoms, but it is the vessels that are the main object to be examined by transcranial imaging.

The proposed basic version of the transcranial phantom facilitates learning primary coordination skills, while the anatomical version simulates a clinical situation. We believe that, with due consideration of the above drawbacks, the design process and the phantoms themselves may be useful for the training of medical sonographers. The developed phantoms may be used for research purposes, for example, for the development of promising imaging modes and teaching transcranial ultrasonography in medical schools as part of training and education of healthcare professionals. The latter requires methodological support, which is under development now. Metal objects in the anatomical version of the phantom may serve to simulate shrapnel [16] left after the mine explosions in the bodies of people who live or work in war areas; therefore, the phantom can be used to assess the magnetically induced shrapnel displacement and the resulting tissue and vascular damage.

In the future, we plan to ensure the ergonomics of the anthropomorphic phantom by using a special stand and magnetic fasteners for the phantom sections, to make the sensations during the study more realistic by modeling the skin, and to supplement the phantom with a vascular blood flow model to provide an opportunity for Doppler ultrasound practice.

Although the presented phantoms were developed for diagnostic purposes, the anatomical version can be adapted for testing of high-intensity ultrasound surgeries. In this case, a part of the skull through which the ultrasonic waves will pass should be made of photopolymer resin as this material adequately models the acoustic properties of bone tissue, as shown in our study, and the space between the brain and the skull models should be filled with a sound-conductive gel.

## Conclusion

1. A basic version of the anthropomorphic training phantom for transcranial ultrasonography has been developed. The skull model has been derived from a CT scan. The acoustic window is made of photopolymer resin, the rest of the skull is printed from PLA plastic, and the brain substance is made of plastisol and zinc oxide mixture. Pins

are inserted into the brain-mimicking substance, forming a specific pattern that can be used for navigation when practicing transcranial ultrasound imaging.

2. An anatomical version of the phantom has been developed, comprising a realistic model of the brain obtained from magnetic resonance imaging data. The brain model contains simulated shrapnel-induced injuries mimicked by adding plastic, metal, and bone-tissue objects of 1 to 3 mm to the tissue-mimicking material. The objects have been mapped by computed tomography, which can be useful for navigation during ultrasound examination of the phantom.
3. Using the STL files posted online [14] and following the described fabrication procedure, anyone can independently reproduce the proposed phantom versions to teach and train healthcare professionals and to develop and improve transcranial ultrasound imaging algorithms.

**Acknowledgements** The authors gratefully acknowledge valuable advice from Igor Demin (PhD, Associate Professor, UNN), Igor Sokolov (Dr.Sci, MPEI) and Georgy Grigoriev (PhD), and thank Albina Laipan (junior researcher, Moscow Radiology) for help in obtaining data. Assistance with editing the manuscript provided by Marina Vlasova was also highly appreciated. The research leading to these results received funding from the Moscow Healthcare Department as part of the Program “Scientific Support of the Capital’s Healthcare” for 2020–2022 under Grant Agreement No. AAAA-A20-120071090054-9.

## Declarations

**Conflict of interest** The authors do not have any conflicts of interest to declare.

## References

1. Walter U, Kanowski M, Kaufmann J, Grossmann A, Benecke R, Niehaus L (2008) Contemporary ultrasound systems allow high-resolution transcranial imaging of small echogenic deep intracranial structures similarly as MRI: a phantom study. *Neuroimage* 40:551–558. <https://doi.org/10.1016/j.neuroimage.2007.12.019>
2. Bock M (2015) MRI compatible head phantom for ultrasound surgery. *Ultrasonics* 57:144–152. <https://doi.org/10.1016/j.ultras.2014.11.004>
3. Eames MDC, Farnum M, Khaled M, Elias WJ, Hananel A, Snell JW, Kassell NF, Aubry J-F (2015) Head phantoms for transcranial focused ultrasound. *Med Phys* 42:1518–1527. <https://doi.org/10.1118/1.4907959>
4. Culjat MO, Goldenberg D, Tewari P, Singh RS (2010) A review of tissue substitutes for ultrasound imaging. *Ultrasound Med Biol* 36:861–873. <https://doi.org/10.1016/j.ultrasmedbio.2010.02.012>
5. Cabrelli LC, Pelissari PI, Deana AM, Carneiro AA, Pavan TZ (2017) Stable phantom materials for ultrasound and optical imaging. *Phys Med Biol* 62:432–447. <https://doi.org/10.1088/1361-6560/62/2/432>
6. Mackle EC, Shapey J, Maneas E, Saeed SR, Bradford R, Ourselin S, Vercauteren T, Desjardins AE (2020) Patient-specific polyvinyl alcohol phantom fabrication with ultrasound and X-Ray contrast for brain tumor surgery planning. *J Vis Exp* 161. <https://doi.org/10.3791/61344.10.3791/61344>
7. Purkayastha S, Sorond F (2012) Transcranial Doppler ultrasound: technique and application. *Semin Neurol* 32:411–420. <https://doi.org/10.1055/s-0032-1331812>
8. Fry FJ, Barger JE (1978) Acoustical properties of the human skull. *J Acoust Soc Am* 63:1576–1590. <https://doi.org/10.1121/1.381852>
9. Kremkau W, Barnes RW, McGraw CP (1981) Ultrasonic attenuation and propagation speed in normal human brain. *J Acoust Soc Am* 70:29–38. <https://doi.org/10.1121/1.386578>
10. Matheo LL, Geremia J, Calas MJG, Costa JFS, Silva FFF, Krüger MA, Pereira WCA (2018) PVC-based anthropomorphic breast phantoms containing structures similar to lactiferous ducts for ultrasound imaging: a comparison with human breasts. *Ultrasonics* 90:144–152. <https://doi.org/10.1016/j.ultras.2018.06.013>
11. Carvalho IM, Matheo LL, Silva JF, Costa JFSC, Borba CM, Krüger MA, Infantosi AFC, Pereira WCA (2016) Polyvinyl chloride plastisol breast phantoms for ultrasound imaging. *Ultrasonics* 70:98–106. <https://doi.org/10.1016/j.ultras.2016.04.018>
12. Osipov LV, Kulberg NS, Skosyrev SV, Leonov DV, Grigoriev GK, Vladimirovskiy AV, Morozov SP (2021) Transcranial beam steering with aberration correction. *Biomed Eng* 54:438–442. <https://doi.org/10.1007/s10527-021-10057-3>
13. Leonov DV, Kulberg NS, Yakovleva TV, Solovyova PD (2022) Approach to detecting aberrations in transcranial ultrasound imaging. *Acoust Phys* 68:175–186. <https://doi.org/10.1134/S106377102202004X>
14. STL files for 3D printing the ultrasound head phantom. [https://www.researchgate.net/publication/355882487\\_Ultrasound\\_head\\_phantom](https://www.researchgate.net/publication/355882487_Ultrasound_head_phantom)
15. Leonov DV, Kulberg NS, Gromov AI, Morozov SP, Kim SY (2018) Causes of ultrasound doppler twinkling artifact. *Acoust Phys* 64:105–114. <https://doi.org/10.1134/S1063771018010128>
16. Kanj A, Ghosn I, Mohanna A, Rouhana G (2021) What radiologist should know about MRI translational forces and hazard: an ex-vivo simulation of retained metallic shrapnel. *Radiol Res Pract*. <https://doi.org/10.1155/2021/6672617>

**Publisher’s Note** Springer Nature remains neutral with regard to jurisdictional claims in published maps and institutional affiliations.